Low Human-Effort, Device-Free Localization with Fine-Grained Subcarrier Information

Ju Wang, Jie Xiong, Hongbo Jiang, *Senior Member, IEEE*, Kyle Jamieson, Xiaojiang Chen, Dingyi Fang, and Chen Wang, *Member, IEEE*

Abstract—Device-free localization of objects not equipped with RF radios is playing a critical role in many applications. This paper presents LIFS, a Low human-effort, device-free localization system with fine-grained subcarrier information, which can localize a target accurately without offline training. The basic idea is simple: channel state information (CSI) is sensitive to a target's location and thus the target can be localized by modelling the CSI measurements of multiple wireless links. However, due to rich multipath indoors, CSI can not be easily modelled. To deal with this challenge, our key observation is that even in a rich multipath environment, not all subcarriers are affected equally by multipath reflections. Our CSI pre-processing scheme tries to identify the subcarriers not affected by multipath. Thus, CSI on the "clean" subcarriers can still be utilized for accurate localization. Without the need of knowing the majority transceivers' locations, LiFS achieves a median accuracy of 0.5 m and 1.1 m in line-of-sight (LoS) and non-line-of-sight (NLoS) scenarios, respectively, outperforming the state-of-the-art systems.

Index Terms—Device-free localization, channel state information, low human-effort, multipath

1 Introduction

We have witnessed an ever-increasing roll-out of location-based applications, such as indoor localization [1], [2], shop navigation [3], [4], etc, for which location information is the key. Most current localization systems, however, require the person to carry a device (such as a mobile phone), making them a poor fit for some applications. For instance, in intrusion detection [5], [6], expecting an uncooperative target to carry a device is not realistic. In elderly care, the aged are reluctant to wear a wearable device or bring a mobile [7]. As such, device-free localization without any device attached to the target has attracted a lot of research efforts recently [8], [9].

Among all the technologies employed for indoor localization, Wi-Fi is still considered one of the most promising schemes due to its ubiquity. For example, more smart/wearable devices equipped with Wi-Fi chips are available in the modern offices and home environments. These smart devices together with mobiles, laptops, smart refrigerators, smart TVs, etc. provide us more Wi-Fi links. Ideally, we want to passively localize a target with only these existing Wi-Fi links without any additional infrastructure.

Traditional device-free localization systems (or approaches) are mainly based on the coarse-grained received signal strength (RSS) signatures [6], [10], [11], resulting in a limited localization accuracy [5], [12], [13]. To improve accuracy, fine-grained CSI fingerprint[1]-based systems have been proposed recently [14], [15]. In order to achieve a high localization accuracy, these systems (i) need a comprehensive site survey to build the detailed fingerprint database, and (ii) require updating the database from time to time because in a real indoor environment, the radio-frequency (RF) signals vary due to environmental changes. The site survey and frequent database update incur a prohibitively-high human cost, rendering them impractical for real-life deployment. These existing systems also assume that all the transceivers' locations are known and remain unchanged. They will encounter large localization errors if the locations of transceivers (such as mobile phones) change, since the change of a Wi-Fi link would lead to the fingerprints in the database not matching the measured CSI readings.

On the other hand, raw CSI measurements from COTS devices can not be directly applied to model a target's location because of strong multipath propagations and hardware noise. Thus, the previous approaches [14], [15] have difficulties employing a unified model to accurately quantify relationship between the CSI measurement and the target's location. As a result, they require a significant amount of

- J. Wang, X. Chen, and D. Fang are with the School of Information Science and Technology, Northwest University, China. E-mail: {wangju, xjchen, dyf}@nwu.edu.cn.
- J. Xiong is with the College of information and Computer Sciences, University of Massachusetts-Amherst, Amherst, MA 01003. E-mail: jxiong@cs.umass.edu.
- H. Jiang is with the College of Computer Science and Electronic Engineering, Hunan University, Changsha, Hunan 410006, China. E-mail: hongbojiang2004@gmail.com.
- K. Jamieson is with the Department of Computer Science, Princeton University, Princeton, NJ 08544 and University College London, London WC1E 6BT, United Kingdom. E-mail: kylej@cs.princeton.edu.
- C. Wang is with the School of Electronic Information and Communications, Huazhong University of Science and Technology, Wuhan, Hubei 430074, China. E-mail: cwangwhu@gmail.com.

Manuscript received 13 Sept. 2016; revised 27 Sept. 2017; accepted 15 Feb. 2018. Date of publication 12 Mar. 2018; date of current version 1 Oct. 2018.
(Corresponding author: Xiaojiang Chen.)
For information on obtaining reprints of this article, please send e-mail to: reprints@ieee.org, and reference the Digital Object Identifier below.
Digital Object Identifier no. 10.1109/TMC.2018.2812746

1. A fingerprint is a unique feature of the signal related to the location, such as RSS or CSI.

human efforts to manually build and update a fingerprint database frequently. If we can quantify the relationship between the target location and the CSI measurement with a model, many applications would benefit, bypassing the labor-intensive training process. In intruder tracking scenario, we can localize the intruders in an unfamiliar scenario that is not likely to have a pre-obtained fingerprint database.

In this paper, we present LiFS, an accurate model-based device-free localization system with low human effort. LiFS does not rely on an exhaustive fingerprint database and only requires baseline measurements between transceivers. That is to say, the amount of human efforts for LiFS is very small compared with measuring or updating the RSS/CSI signatures at all possible locations in existing fingerprint-based location systems. Without knowing the locations of all transceivers, LiFS is able to achieve a high localization accuracy (sub-meter level), while most existing device-free localization systems exhibit a coarse accuracy. Many real-life applications would benefit from the sub-meter level localization accuracy. For example, for the location-oriented activity identification system, a 2 m localization error would lead the system to wrongly detect cooking activity as washing dishes [16].

To remove the noise on raw CSI measurements, we observe that not all subcarriers are affected equally by multipath. Consequently, we introduce a novel CSI pre-processing method to filter out those subcarriers greatly affected by multipath and hardware noise. After this processing, we can quantify the relationship between the pre-processed CSI values and a target's locations with the help of a power fading model (PFM).[2] With such a relationship, LiFS can calculate a target's location without requiring any labor-intensive offline training.

LiFS still faces the challenge that the locations of some transceivers (such as mobile phones, laptops, etc.) are unknown, since a target's location estimate is related to the transceivers' locations in the PFM. To address this challenge, LiFS establishes a set of equations with the help of the PFM to restrict the locations of both the target and the transceivers with unknown locations. *The key observation is that the number of unknown transceivers grows linearly while the number of PFM equations grows in a quadratic fashion*. This implies that with enough Wi-Fi links, the equation constraints will be sufficient to localize both the unknown transceivers and the target.

To illustrate the idea of LiFS, Fig. 1 shows a toy example with one target and five transceivers (i.e., three APs, one mobile phone and one laptop). We assume the mobile's location is unknown, so the total number of unknowns is four since both the mobile and the target have two unknown parameters, namely their $[x, y]$ coordinates in 2D space. The total number of Wi-Fi links is six (3×2) so we can establish six PFM equations. Thus there are enough constraints to localize the target and the mobile phone in this example.

Although the idea sounds straightforward, it is non-trivial to solve the PFM equations efficiently due to the complex non-linear Fresnel integration in PFM [17]. To handle this, we seek an optimization solution that minimizes the mean absolute error between the CSI measurements and the PFM-calculated CSI values. To this end, we use a hybrid approach that starts with the genetic algorithm (GA) [18] by picking an initial set of solutions[3] efficiently without a local minima, and then refine the solution employing the gradient descent (GD) [19] scheme to reach the final location estimate. We also propose LiFS-A scheme which employs the simplified PFM equations for occasions when users demand low latency rather than high accuracy.

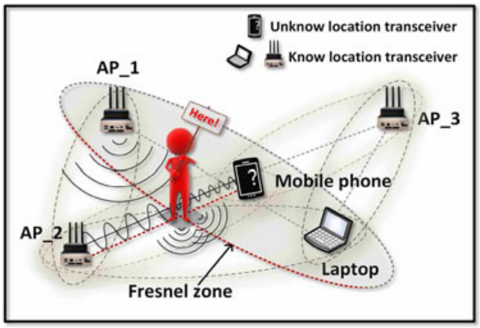

Fig. 1. A toy example of localization with LiFS.

We build a prototype of LiFS and LiFS-A employing 11 laptops, each equipped with an Intel 5300 NIC [20]. Four of them serve as access points (APs) with the "hostapd" tool [21], and the rest serve as clients. Note that we do not include the links between clients as we only assume access to CSI data from APs. The target to be passively localized is a human without any device attached. Our experimental results demonstrate that, even in a challenging situation when the locations of 6 out of all the 7 clients are unknown, LiFS achieves a median accuracy of 0.5 m and 1.1 m in LoS and NLoS scenarios respectively for a single target, outperforming the state-of-the-art systems. The localization error of the LiFS-A increases slightly, however the time cost reduces 80 percent compared with LiFS. For two targets, LiFS can still localize each individual target accurately when the targets are 1.8 m apart. Note that passively localizing more than one target is a well-known challenging problem [12].

Contributions. The main contributions are as follows:

1) We propose a novel CSI pre-processing scheme to select those "clean" subcarriers, which conform to the proposed model, thus ensure a high localization accuracy even in rich multipath environment.
2) By modelling the device-free localization problem as a set of over-determined equations, LiFS does not need to know the locations of all the transceivers and determines their locations together with the target.
3) We simplify the LiFS to reduce the time cost by approximating fading model and adopting the least squares method, so that the system can be appropriate for the occasion when users demand low time cost rather than high location precision.
4) LiFS is implemented on commercial off-the-shelf hardware and extensive experiments demonstrate the effectiveness of the system.

2. The power fading model [17] describes the relationship between the power fading, i.e., the CSI amplitude, and the distances between the target and the two transceivers.

3. A solution consists of a vector of all the unknowns, i.e., the locations of a target and the transceivers with unknown locations.

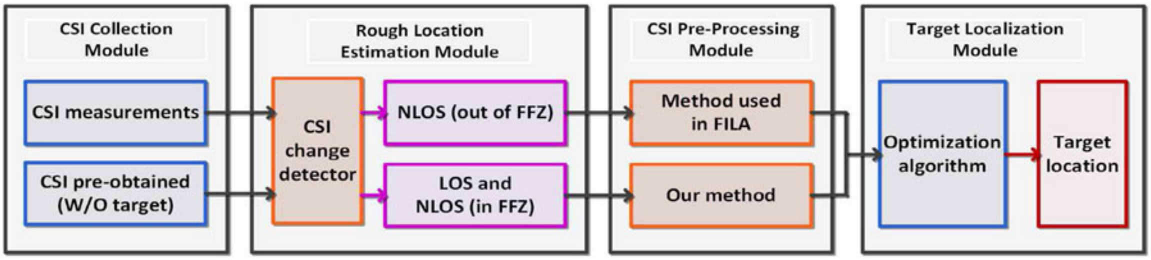

Fig. 2. System overview of LiFS.

2 Related Work

There are growing interests in exploring RF for device-free localization. Compared with camera or infrared based solutions [22], [23], RF-based device-free localization approaches can work at day and night, and also can penetrate non-metallic walls [12]. Recently, multiple fine-grained RF-based localization systems have been proposed, such as Wi-Vi [24], WiDeo [25], Witrack2.0 [8], mTrack [26], and Tadar [9]. Although achieving high accuracies, these methods either require exsepneive dedicated hardware, such as USRPs to send out special-purse frequency modulated carrier wave (FMCW) signal [8] not compatible with the current 802.11 Wi-Fi protocol or employ high frequency 60 GHz signals [26] or customized RFID readers with a tag array [9]. In contrast, our LiFS system builds upon the commercial off-the-shelf hardware, making it a promising candidate for real-life deployment.

On the other hand, several RSS-based device-free localization systems have been proposed [5], [6], [10], [12], [13], [27], [28], achieving the goal of low hardware cost for localization as RSS readings are widely available in commercial off-the-shelf Wi-Fi devices. For example, ACE [27] can even localize multiple targets based on the RSS measurements of a large number of Wi-Fi transceivers deployed around the monitoring area. However, RSS is inherently a coarse measurement [29] and strong multipath makes the performance even worse [30]. As such, RSS-based device-free localization techniques have difficulties providing high localization accuracies [8], [14], [31].

Compared with RSS, CSI measurements provide more fine-grained information on each subcarrier with both amplitude and phase information for device-free detection and localization [14], [15], [32]. To localize a target, many systems utilize the CSI measurements as unique signatures of a target's locations [14], [15]. However, these systems suffer from labor-intensive offline training since they need a comprehensive site survey to build and update the fingerprint database. LiFS does not need any training effort, and only requires the baseline measurements between transceivers which is a very small workload.

Additionally, most existing device-free localization proposals including RSS-based [5], [6] and CSI-based [14], [15] rely on the assumption that the locations of all transceivers are known and unchanged. In reality, this assumption could be easily violated since users may move their devices. With enough transceiver pairs, LiFS can determine the locations of both the unknown transceivers and the target, eliminating the necessity of knowing all the transceivers' locations.

Finally, comparing with our conference paper [33], [34], this paper proposes LiFS-A scheme which reduces the complexity of the localization model for occasions when users demand low latency rather than high accuracy.

3 System Overview

LiFS is a model-based device-free localization system that can localize a target with low human effort. LiFS acquires CSI measurements from the existing Wi-Fi infrastructure, and assumes the locations of APs are known. LiFS does not need to know the locations of all the clients (e.g., mobiles) involved for locating a target, and can determine their locations together with the target. LiFS is composed of the following four modules as shown in Fig. 2:

- *CSI Collection Module:* Before the target moves into the monitoring area, LiFS collects a set of CSI measurements (i.e., baseline data) from all the links. LiFS then acquires another set of CSI measurements from all the links when a target moves into the area.
- *Rough Location Estimation Module:* LiFS detects whether the target is present in the First Fresnel Zone (FFZ) of a specific link by comparing the currently measured CSI value with the pre-obtained CSI measurement (i.e., the baseline data).
- *CSI Pre-Processing Module:* If the target is located in FFZ of a specific link, LiFS pre-processes the raw CSI measurements with the scheme introduced in Section 5; otherwise, LiFS uses the scheme proposed in FILA [30] to pre-process the measurements.
- *Target Localization Module:* For each link, LiFS formulates a PFM equation with the pre-processed CSI measurement. By solving a set of PFM equations formulated for all the links, LiFS can estimate the target location accurately as described in Section 6.

4 Background

4.1 Channel State Information Measurement

Most modern digital radios use OFDM communication and transmit signals across orthogonal subcarriers at different frequencies [35], [36]. Each transmitted symbol $X(f)$ is modulated on a subcarrier index f, and the received symbol $Y(f)$ depends on the wireless channel $H(f)$:

$$Y(f) = H(f) \times X(f). \tag{1}$$

The channel matrix $\mathbf{H} = \{H(f)\}_{f=1,\ldots,K}$ is called the *channel state information*, where K is the number of subcarriers. Each $H(f) = |h_f|e^{\mathbf{J}\cdot\theta_f}$ is a complex value depicting the changes of the amplitude $|h_f|$ and the phase θ_f between transmitter and receiver at subcarrier f, where $\mathbf{J}$ is the

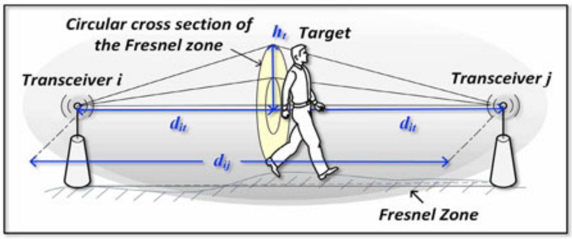

Fig. 3. Power fading model.

imaginary unit. That is to say, the CSI amplitude measures the power fading of the Wi-Fi link between the transmitter and the receiver. For each transmission, a group of CSI measurements on $K = 30$ subcarriers are exported by leveraging a COTS Intel 5300 NIC with a public driver [20], [29].

4.2 Power Fading Model

To localize a target, we need to understand the effect of a target's location on the CSI measurement. Let λ denote the wavelength of the wireless signal and we use the location vector $C = [x, y]$ to describe the 2D coordinate. Then, the coordinates of the transmitter i, receiver j and the target are referred to as C_i, C_j and C_t, respectively. Then the wireless link ℓ_{ij} between transmitter i and receiver j has a length of $d_{ij} = \sqrt{(C_i - C_j)^T(C_i - C_j)}$. Similarly, we can calculate d_{it} and d_{jt}, which are the distances from the target to the transmitter i and the receiver j. According to wireless communication principles [17], the power fading between the two transceivers is mainly related to the *propagation fading*, *diffraction fading* and *target absorption fading*.

Propagation Fading. Propagation fading L_{ij} specifies the attenuation due to propagation of a distance d_{ij} between the transmitter i and the receiver j [17] as follows in dBm:

$$L_{ij} = 10 \log [\lambda^2/(16\pi^2 d_{ij}^2)]. \tag{2}$$

Diffraction Fading. Diffraction fading D_{ijt} specifies the attenuation due to a target located in the First Fresnel Zone (FFZ) of link ℓ_{ij} [17]. A Fresnel zone is an ellipsoid whose foci are the transmitter and the receiver, as shown in Fig. 3. The radius of the circular cross section of the FFZ is given by $r_1 = \sqrt{(\lambda \cdot d_{it} \cdot d_{jt})/d_{ij}}$. The diffraction fading is significant when a target is located within the FFZ; while the diffraction fading is very small when the target is far away from the FFZ [17]. D_{ijt} is a function of the distances from the target to transmitter i and receiver j, which is given by:

$$D_{ijt} = 20 \log \left(\frac{\sqrt{2}}{2} \cdot \left| \int_v^\infty \exp(\frac{-\mathbf{J} \cdot \pi z^2}{2}) dz \right| \right), \tag{3}$$

where $v = h_t \sqrt{2(d_{it} + d_{jt})/(\lambda \cdot d_{it} \cdot d_{jt})}$ determines the volumes of the diffraction fading, and h_t is the target's effective height. h_t is defined as the distance from the highest point of the target to the wireless link.

Equation (3) shows that we need to know the effective height in order to localize the target. Fig. 3 describes an ideal example where the heights of the two transceivers are the same. In this case, the effective height is a constant wherever the target is located. However, the heights of transceivers will be different in reality. As a result, the effective height is always changing when a target is located at different locations. Since the target location is an unknown, it is impossible to predict the effective height beforehand. We present our solution to handle this "changing effective height" problem in Section 6.

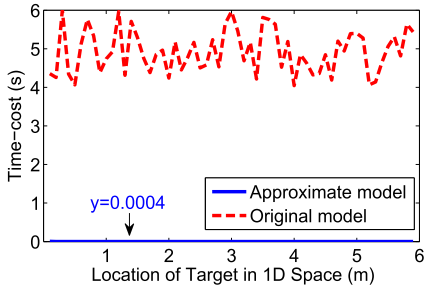

Fig. 4. The calculation time of diffraction fading model.

Target Absorption Fading. When a target is located exactly on the LoS path, a link suffers large extra signal attenuation absorbed by the target, which is denoted as A_t ($A_t < 0$) and is dependent on the target.

Putting things together, when a target is located in the monitoring area, the power fading between the transmitter i and the receiver j, i.e., the CSI amplitude[4] measurement R_{ij}, is expressed as below in dBm:

$$R_{ij} = \begin{cases} L_{ij} + D_{ijt} + A_t + \eta, \ LoS, & (4) \\ L_{ij} + D_{ijt} + \eta, \ NLoS \ but \ still \ in \ FFZ, & (5) \\ L_{ij} + \eta, \ \ outside \ of \ FFZ, & (6) \end{cases}$$

where η is the measurement noise. "NLoS but still in FFZ" in Eqn. (5) means that the target is not on the LoS path but still located in FFZ. We refer Eqns. (4), (5), and (6) as the power fading model and rewrite them as R_{ij}=$PFM(C_i, C_j, C_t, h_t)$. For simplicity, we use "CSI" to represent "CSI amplitude" in the rest of this paper.

4.3 Approximate Model of Fresnel Integration

In Eqn. (3), $F(v) = \frac{\sqrt{2}}{2} \cdot |\int_v^\infty \exp(\frac{-\mathbf{J} \cdot \pi z^2}{2}) dz|$ is a complex Fresnel integration which is difficult to calculate, because the integrand contains a complicated exponential function. Thus we apply a approximation given by Lee [37] to simplify the Eqn. (3) as:

$$D = \begin{cases} 0 & \mathrm{v} < -1 \\ 20 \log (0.5 - 0.62\mathrm{v}) & -1 \le \mathrm{v} \le 0 \\ 20 \log (0.5 exp(-0.95\mathrm{v})) & 0 \le \mathrm{v} \le 1 \\ 20 \log (0.4 - \sqrt{0.12 - (0.38 - 0.1\mathrm{v})^2}) & 1 \le \mathrm{v} \le 2.4 \\ 20 \log (\frac{0.225}{\mathrm{v}}) & \mathrm{v} > 2.4. \end{cases} \tag{7}$$

We now conduct a simulation to verify the calculation time of the approximation model decreases. The Fig. 4 shows the results when the distance between transmitter i and target is 0.1 m to 5.9 m. The calculation time of original diffraction fading model and the approximation model are 4 s to 6 s and 10^{-4} s respectively. The result is that the calculation time decreases 99.99 percent.

4. Note that the Intel 5300 NIC reports the CSI amplitude in voltage space [20]. We convert the amplitude of CSI $|h|$ into R with the unit of dBm as: $R = 20\log(|\mathrm{h}|/1000)$.

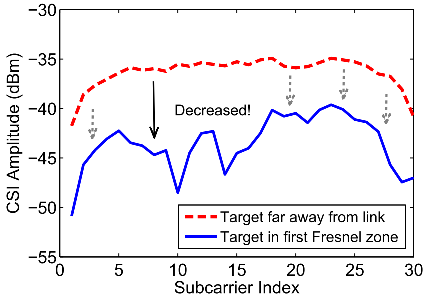

Fig. 5. CSI measurements in an outdoor open space with and without a target located in FFZ.

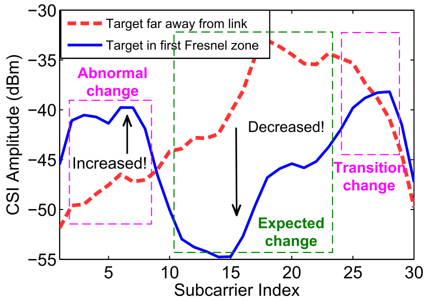

Fig. 6. CSI measurements in a typical office room with and without a target located in FFZ.

5 Pre-Processing CSI Measurement

For a given deployment setup, the power fading model shows that the CSI change is only related to a target's location and the effective height when the target is located inside the FFZ. However, strong multipath reflections and environmental noise [14], [15] may also affect the CSI change. We would like to filter out those subcarriers greatly affected by multipath and noise, thus only retrieving the CSI changes on the "clean" subcarriers for our location estimate.

5.1 CSI Change in Multipath Environment

To understand the CSI changes in rich multipath environment, we conduct experiments in both an outdoor open space and a typical indoor office room. In each environment, an AP acts as the transmitter and a laptop equipped with Intel 5300 NIC is employed as the receiver. We set the distance between the transmitter and the receiver as 6 m and place the two transceivers at the same height in order to eliminate the impact of height difference. In each environment, we collect two sets of CSI measurements when a target is located inside and outside the FFZ, and the results are shown in Figs. 5 and 6, respectively.

Fig. 5 illustrates that the CSI amplitudes of all the subcarriers are decreased in the open space environment when a target is located in the FFZ, which is consistent with the diffraction theory [17]. However, in the indoor office environment, the situation is more complicated. Fig. 6 displays that the CSI amplitudes of some subcarriers are increased (e.g., the 5th subcarrier) or remain unchanged (e.g., the 9th subcarrier), which are obviously inconsistent with the diffraction theory. Thus, if we apply the power fading model directly on the raw CSI measurements, these inconsistencies will result in large localization errors. For example, Fig. 7 shows the CSI changes of all subcarriers when we let a target move along the LoS path from the transmitter to the receiver. For evaluation purposes, we also plot the theoretical CSI values in Fig. 7 based on the diffraction theory in Eqn. (3). We can see that the variations of the raw CSI change measurements are quite large, and the averaged values do not match the theoretical curve well.

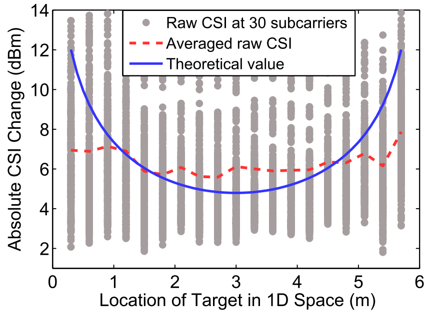

Fig. 7. CSI changes at 30 subcarriers when a target is located at different locations.

The CSI changes at all subcarriers in an indoor environment can be categorized into three groups which we term them as *expected change*, *abnormal change* and *transition change* shown in Fig. 6. The *expected change* has a feature similar to the outdoor open space environment, which is mainly caused by the presence of a target and conforms to the diffraction theory. The *abnormal change* has an opposite effect to the *expected change*, i.e., the CSI amplitude is increased rather than decreased. This *abnormal change* is caused by constructive multipath propagations in the indoor environment. The *transition change* is the "transition zone" between the *expected change* and the *abnormal change*.

5.2 Pre-Processing Scheme for CSI

The intuition of the pre-processing scheme is that different subcarriers are experiencing frequency-selective fading [38]. Thus, not all subcarriers are affected equally by the multipath as depicted in Fig. 6. Our objective is to remove those subcarriers greatly affected by multipath because the CSIs on these subcarriers do not fit the theoretical model. To filter out these *dirty subcarriers* with abnormal CSI changes, our first step stems from the "power increase" observation at some subcarriers. Specifically, when the CSI amplitude of the kth subcarrier is increased instead of decreased, we know the subcarrier is affected by multipaths and the CSI measurement at this subcarrier should be filtered out. Unfortunately, it is not easy to filter out the *transition part* since it may also exhibit the "power decrease" feature. To address this issue, we adopt a threshold to filter out the subcarriers in the transition part based on whether the power decrease is large enough. Specifically, if a target is not located on the LoS path, the threshold δ_{eff} is defined as the averaged standard deviation over all the K subcarriers:

$$\delta_{eff} = \frac{1}{K}\sum_{k=1}^{K}\frac{f_k}{f_0} \times \delta_k, \tag{8}$$

where f_0 is the central frequency, f_k is the frequency of kth subcarrier, and δ_k is the standard deviation of the amplitudes of baseline CSI measurements on kth subcarrier when no target is present. A large number of baseline CSI readings is helpful for an accurate δ_k estimation. However, it incurs a high latency. In our experiments, we find 100 CSI readings are good enough and it takes 10 s when we employ beacons

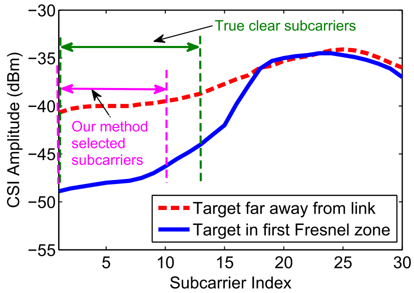

(a) Target stands at LoS "location 1".

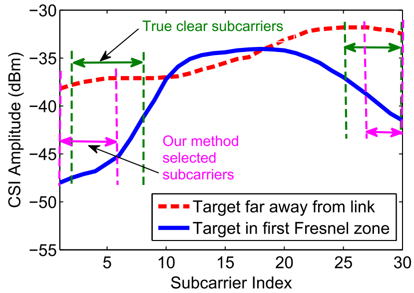

(b) Target stands at LoS "location 2".

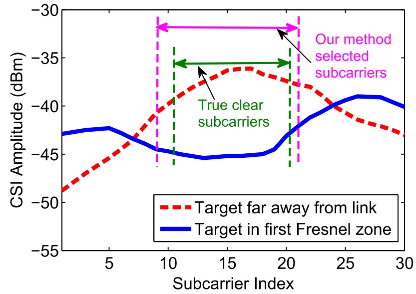

(c) Target stands at NLoS "location 3".

Fig. 8. CSI amplitudes of all the subcarriers when a target is located inside the FFZ at three different locations.

with 100 ms interval. Note that the different weighting factors $\frac{f_k}{f_0}$ is based on the fact that radio propagation is frequency-dependent [30]. If a target is located on the LoS path, the threshold δ_{eff} should be added with the absolute signal attenuation $|A_t|$ caused by the target. To identify whether a target is located on the LoS path, the key observations are (i) $|A_t|$ is usually within the range of 4–9 dBm [10], [13], [39] when a human target blocks the LoS path, and (ii) the noise is usually within 1–3 dBm [12], [40]. Thus, a target is more likely located on the LoS path if the averaged CSI change of all subcarriers is larger than 5 dBm. Unless specifically mentioned, we denote δ_{eff} as the threshold for simplicity in the rest.

Let $\mathbf{F} = \{F_1, F_2, \ldots, F_K\}$ be the CSI measurements when a target is inside the FFZ of a link, and $\mathbf{O} = \{O_1, O_2, \ldots, O_K\}$ be the baseline CSI measurement acquired when we make sure there is no target present in the monitoring area. I is a set of subcarrier indices in which the CSI amplitude decrease is larger than the threshold δ_{eff}, i.e., $I = \{j : |F_j - O_j| > \delta_{eff}, 1 \leq j \leq K\}$. When a target appears, the *effective CSI* value CSI_{eff} and the *effective CSI change* value ΔCSI_{eff} are calculated as:

$$CSI_{eff} = \frac{1}{|I|}\sum_{j\in I}\frac{f_j}{f_0} \times F_j, \tag{9}$$

$$\Delta CSI_{eff} = \frac{1}{|I|}\sum_{j\in I}\frac{f_j}{f_0} \times |F_j - O_j|. \tag{10}$$

We emphasize that the effective CSI CSI_{eff} is the desirable output of the pre-processing scheme. If a target is located on the LoS path, CSI_{eff} should conform to Eqn. (4), otherwise it should conform to Eqn. (5). The effective CSI change ΔCSI_{eff} should conform to the diffraction fading D in Eqn. (3). Obviously, if ΔCSI_{eff} matches the model-calculated D well, the power fading model can be applied to estimate a target's location accurately. Note that we have CSI from 30 subcarriers and as long as a few of them fall in the *clean* category, it is enough for our localization purposes. In the future, we will improve the accuracy of selecting the clean subcarriers with the help of phase information. For example, multiple adjacent subcarriers should exhibit a linear phase change if these subcarriers are clean. However, the phase information obtained from COTS Wi-Fi devices is very noisy [41] and can not be applied directly.

5.3 CSI Pre-Processing Scheme Verification

Under the same deployment setup described in Section 5.1, we conduct experiments in three different environments, i.e., a library, an office and an indoor empty hall corresponding to high, medium and low multipath scenarios. Due to space limitations, we only show the experimental environment of the indoor office in Fig. 9. In all three environments, we set the distance between the laptop and the AP to be 6 m. The following three claims validate the effectiveness of our pre-processing scheme.

Claim 1. The CSI pre-processing scheme removes the subcarriers which are greatly affected by multipath and preserves those relatively "clean" CSI measurements which are not affected by multipath much.

To verify the effectiveness of our scheme in identifying the "clean" subcarriers, we acquire ground truth with the help of CSI measurements in an outdoor open space which has very little multipath. We make sure the link length and the relative target location are the same in both outdoor open space and indoor environment. First, in the outdoor open space, we obtain a relatively stable and constant CSI change at all the subcarriers because of little multipath. Then, in the indoor environment, we identify the subcarriers with CSI changes close to the stable change in the outdoor open space as the "clean" subcarriers.

Figs. 8a, 8b, and 8c show the CSI amplitudes of all the subcarriers when a human target is located at three different locations in the office. The three locations are randomly selected within the FFZ. Specifically, the "location 1" and "location 2" are two locations along the LoS path and the "location 3" is a location on a NLoS path but still in the FFZ. The mean and standard deviation of the CSI changes over all the subcarriers in Fig. 5 are 7.25 dBm and 2.02 dBm, respectively. Due to the environmental and hardware noises, we take subcarriers whose CSI changes are within 7.25-2.02 dBm and 7.25+2.02 dBm as the ground truth "clean" subcarriers. Our CSI pre-processing scheme chooses the subcarriers whose CSI decreases are larger than the

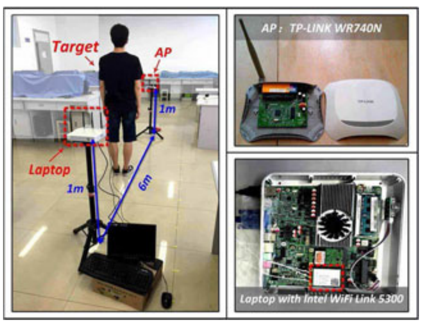

Fig. 9. Experimental environment and deployment setup.

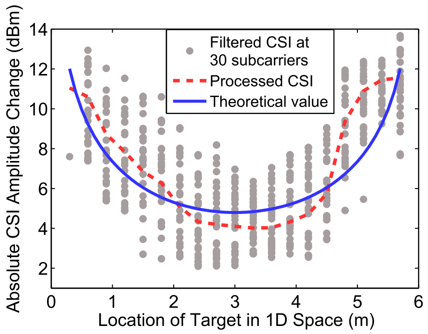

Fig. 10. CSI change measurements after pre-processing.

threshold δ_{eff}. Figs. 8a and 8b show the results when the target is located on the LoS path at two different locations, and Fig. 8c shows the results when a target is located on the NLoS path but still in FFZ. In this experiment, the averaged standard deviation over all subcarriers is 2.82 dBm and the minimum empirical absolute signal attenuation $|A_t|$ caused by the target is 4 dBm. Thus, the threshold δ_{eff} is 6.82=2.82+4 dBm in Figs. 8a and 8b, and 2.82 dBm in Fig. 8c. Based on these thresholds, the results of Figs. 8a, 8b, and 8c show that the subcarriers selected by our pre-processing scheme match the ground truth "clean" subcarriers quite well. Note that, multipath may also cause a signal power decrease on some subcarriers. However, it's challenging to identify these subcarriers as the attenuations caused by the human body vary a lot. We remove those subcarriers definitely affected by multipaths and still keep the rest. Moreover, we input averaged CSI changes of all selected subcarriers into model thus few wrongly selected subcarriers have a small impact on the localization performance.

To summarize, our pre-processing scheme is able to preserve those relatively "clean" CSI measurements which are not affected by multipath much. We only show the results in the office here as the results from the other two environments have a similar trend. Note that the method to obtain ground truth "clean" subcarriers for verification can not be applied to identify the "clean" subcarriers in localization experiments because it requires the link length and target location as the input which are not available. On the other hand, the proposed pre-processing method does not need to know this information.

Claim 2. The pre-processed CSI change measurement matches the diffraction-model-calculated value well.

Fig. 10 shows the pre-processed CSI measurements when a target moves along the LoS path between transmitter and receiver as mentioned in Section 5.1. For each location, we acquire the pre-processed CSI change ΔCSI_{eff} based on Eqn. (10). Compared with the raw CSI measurements which behave quite randomly as shown in Fig. 7, the pre-processed CSI changes are relatively stable and match the model-calculated values well in Fig. 10. We also conducted experiments by varying the distance between the transmitter and receiver from 3 m to 7 m at a step size of 1 m in three different environments. Fig. 11 shows the absolute CSI change errors between the pre-processed CSI change measurements and the diffraction-model-calculated values. We can see that most errors are below 1.5 dBm which is smaller than the reported noise variations (2.82 dBm).

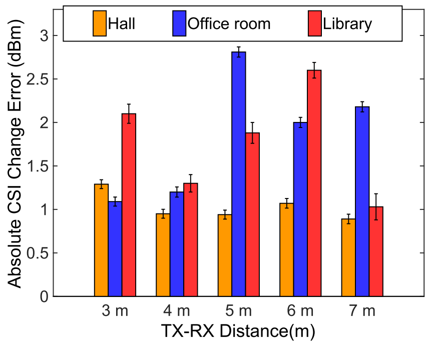

Fig. 11. Absolute CSI change errors under different transmitter-receiver distances.

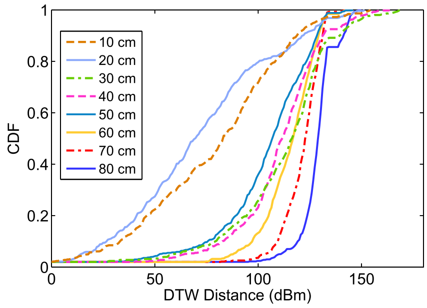

Fig. 12. DTW distances of the pre-processed CSI.

These results show that the pre-processed CSI changes match the diffraction-model-calculated values well.

Claim 3. The pre-processed CSI is a fine-grained spatial indicator.

A fine-grained spatial indicator should have the capability to distinguish a target's small movements. The distinguishing capability is reflected in the dissimilarities of the two CSI measurements. A CSI measurement is a K-dimensional vector whose elements are from K subcarriers rather than a single value. Following Wang et al. [42], we use the dynamic time warping (DTW) distance [43] to calculate the dissimilarities of two CSI measurements when a target is at different locations. The detailed DTW distance calculation refers to [33].

To understand the spatial resolution and the discrimination capability of the pre-processed CSI measurements, we let a person move from a reference position with a step size of 10 cm and compute their respective DTW distance with the reference position over 100 measurements. Fig. 12 shows that the median DTW distance of the pre-processed CSI measurements, when comparing with the result of the raw CSI measurements as shown in Fig. 13, the DTW distances becomes large and distinct. It is large even when the movement distance is 10 cm. Note that it's possible two different pairs of CSIs can have the same DTW distance. However, the probability is very low since the CSI changes are relatively random due to the multipath indoors. Even if two pairs of CSIs have the same DTW distance, we can utilize the DTW distances at nearby locations to differentiate them since it is not likely the DTW distance at nearby locations are same again.

6 System Design

6.1 Basic Idea of LiFS

Suppose there are N APs, M clients and one target, which are randomly located in a 2D monitoring area. The number

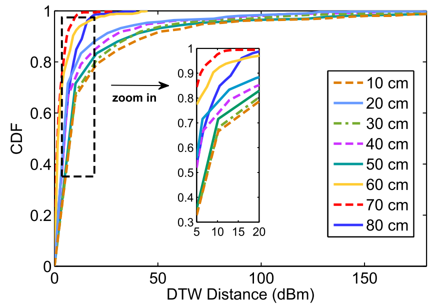

Fig. 13. DTW distances of the raw CSI.

of wireless links between APs and clients is MN. We can also measure a number of $N(N-1)/2$ wireless links between all the APs.[5] Thus, based on the power fading model introduced in Section 4, we can establish a number of $MN + N(N-1)/2$ equations to restrict the location of the target. The locations of APs are fixed and known in reality. Both the target and each of the M clients have two unknown parameters, namely their $[x, y]$ coordinates in the 2D space. As mentioned in Section 4, a target's effective height keeps changing and it is impossible to predict this change. Thus, we also treat the effective height as an unknown. Then, the total number of unknowns is no larger than $2M+3$, since the locations of some clients are known. Note that the number of equations $MN + N(N-1)/2$ grows in a quadratic fashion, while $2M+3$ grows linearly. This suggests that given enough number of clients and APs ($N > 3$), such that $MN + N(N-1)/2 > 2M+3$, there will be enough constraints to determine all the unknown locations of both the target and the unknown clients.

6.2 Location Determination via Optimization

After modelling a set of power fading model equations, LiFS needs to solve these equations to get the target localizations. LiFS solves these equations by attempting to minimize the mean absolute error between the processed CSI data and the power fading model calculated CSI value. More specifically, let $y_{ij} \in Y$ be the pre-processed CSI measurement of the link ℓ_{ij} ($1 \le i \le N$, $1 \le j \le M$). Then our objective function J is given by:

$$J = \min \frac{1}{|Y|} \sum \left| y_{ij} - PFM(C_i, C_j, C_t, h_t) \right|, \qquad (11)$$

where, C_i, C_j and C_t are the locations of APs, clients and the target respectively, and h_t is the target's effective height. We use the wavelength at the center frequency f_0 for calculating the CSI values in power fading model.

LiFS pre-processes y_{ij} with two different schemes. If the target is located in the FFZ of a link, LiFS pre-processes the raw CSI measurement of this link with the scheme introduced in Section 5. Otherwise, LiFS uses the scheme proposed in FILA [30], which is given by:

$$CSI_{eff} = \frac{1}{K} \sum\nolimits_{k=1}^{K} \frac{f_k}{f_0} O_k, \qquad (12)$$

5. Note that we do not consider the links between clients as we only assume access to CSI information from the APs.

where O_k is the CSI measurement of kth subcarrier, f_0 is the central frequency, f_k is the frequency of kth subcarrier and K is the total number of subcarriers.

The principle of selecting pre-processing schemes will be introduced later at the end of this section. Now, we focus on how to solve Eqn. (11). It is noted that J is a non-linear function due to the Fresnel integration. In this case, the gradient descent (GD) algorithm [19] and the genetic algorithm (GA) algorithm [18] are usually employed since they are more efficient than the traditional method. The GD algorithm starting from an initial guess is able to find the closest local minimum. However, the GD algorithm may fail to find a good solution when the number of local minima in J is large. While the GA algorithm can search the solution space more efficiently, it sometimes misses local minima that might provide a reasonably good solution. To gain the benefits of both approaches, motivated by Chintalapudi et al. [44], we use a GA and GD hybrid method to obtain the solutions of all unknowns, i.e., C_j, C_t and h_t to be solved. In each iteration, GA starts picking a set of solutions (initiates all the unknowns) and then refines the solutions via the GD algorithm. Each solution is then evaluated by computing the J value.

If we rewrite the aforesaid objective function as follows:

$$J = \min \frac{1}{|Y|} \sum \left[y_{ij} - PFM(C_i, C_j, C_t, h_t) \right]^2.$$

We observed that this problem is similar to the function $F(x) = \sum f_i^2(x)$ that consists of the quadratic sum of several functions. For this kind of objective function, excepting common methods, there is a more effective approach that can solve it, namely the least squares method. Also, this method has a lower complexity compared with GA and GD, so we can adopt the method to optimize J. Algorithm 1 describes the specific realization process.

Which power fading model formulas should we choose to form the equations? Since the equations in the power fading model are based on the location where the target is located, i.e., LoS, NLoS but still in FFZ, and outside of FFZ. Thus, the power fading model equations are formed with a rough estimation of the target's location. Note that the CSI change is negligible when a target is outside of FFZ while the CSI change is large when a target is on LoS path. Thus, LiFS can estimate the location range of a target roughly based on just the effective CSI changes as below:

$$\begin{cases} |\Delta CSI_{eff}| > |A_t| \Rightarrow LoS\ (in\ FFZ), \\ \delta_{eff} < |\Delta CSI_{eff}| \le |A_t| \Rightarrow NLoS\ but\ still\ in\ FFZ, \\ |\Delta CSI_{eff}| \le \delta_{eff} \Rightarrow outside\ of\ FFZ. \end{cases} \qquad (13)$$

where δ_{eff} ($\delta_{eff} > 0$) is the threshold when no target is present and δ_{eff} can be calculated based on Eqn. (8), and A_t is the target absorption attenuation when the target is located on LoS path. Accordingly, the pre-processing scheme is chosen as follows: (i) The raw CSI values are pre-processed by our scheme in Section 5.2 if the target is located in FFZ; (ii) The raw CSI values are pre-processed by the method proposed in [30] if target is outside of FFZ.

The signal attenuation A_t is dependent on the target so an overweight man may cause a larger signal attenuation than a slim man. To deal with this problem, LiFS takes A_t as an unknown in addition to all the other unknowns. The

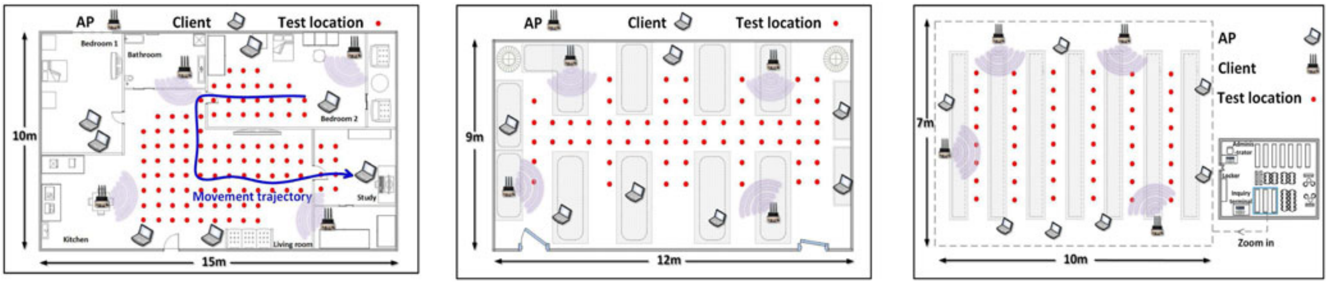

(a) Home with 107 test locations. (b) Classroom with 57 test locations. (c) Library with 48 test locations.

Fig. 14. Experimental floorplan of classroom, home, and library environments.

good thing is that the number of unknowns is usually much smaller than the equations, so one added unknown will not affect the performance of LiFS. To estimate A_t, we first pick an initial value for A_t based on the empirical knowledge. $|A_t|$ is usually within 4–9 dBm [10], [13], [39]. Even if there is a large error in the initial guess for A_t, the optimization scheme is able to reduce the error to a small value after several iterations. For example, in our experiments, the variations of the estimated A_t are no larger than 2 dBm after 3–5 optimization iterations.

Algorithm 1. The Levenberg-Marquardt Method for Nonlinear Least Squares

Input: Diffraction fading: y_{ij}; area of locating: $a \times b$
Output: the coordinate of target $C_t(x, y)$;
within the area $a \times b$, initialize the coordinates of N APs and M clients as C_i and C_j, initialize coordinate of target C_t as x^0 randomly; initialize the target effective height h_t randomly within $[0, 1]$;
let initial parameter $\alpha > 0$, growth factor $\beta > 1$, admissible error $\epsilon > 0$, $r = 0$;
while $r < \mathit{Maximum\ Iterations}$ **do**
  compute $f_m(x^r) = y_{ij} - PFM(C_i, C_j, x^r, h_t)$ $m = 1, \ldots, MN$
  let $f^r = [f_1(x^r), f_2(x^r), \ldots, f_{MN}(x^r)]$, then $F(x^r) = (f^r)^T f^r$;
  calculate partial derivatives of $f(x^r)$, obtaining a matrix $A_r = \begin{bmatrix} \frac{\partial f_1(x^r)}{\partial x} & \frac{\partial f_1(x^r)}{\partial y} \\ \vdots & \vdots \\ \frac{\partial f_{MN}(x^r)}{\partial x} & \frac{\partial f_{MN}(x^r)}{\partial y} \end{bmatrix}$
  while $\| {A_r}^T f^r \| > \epsilon$ **do**
    solve equation $({A_r}^T A_r + \alpha I) d_r = -{A_r}^T f^r$, attaining the orientation vector d_r;
    let $x^{r+1} = x^r + d_r^T$ and compute $F(x^{r+1})$;
    if $F(x^{r+1}) < F(x^r)$ **then**
      $\alpha = \frac{\alpha}{\beta}; r = r + 1; \mathit{break}$;
    else
      $\alpha = \alpha \times \beta$;
    end if
  end while
end while
return $C_t = x^r$

6.3 Coping with Client Mobility

In practice, most clients are mobiles and laptops whose locations may change. However, it is not likely for all users to move their devices simultaneously. By observing the CSI variations of multiple APs, we can filter out the CSI data from moving clients and only keep the data from the static clients. So for a specific client, if multiple APs observe large CSI variations simultaneously, then this client is likely to be moving and the CSI data from this client will not be included for location estimate. Also from our experimental results in Section 8.3.2, we see that even with only one known location client, our system is able to achieve good localization accuracy already.

7 Implementation

Experimental Environments: To verify the effectiveness of LiFS, we conduct experiments in three different environments. The first is a typical home environment with a size of 10 m $\times$ 15 m. It has furniture and obstacles in the form of concrete walls and glass/metal doors. The second environment is an indoor classroom with a size of 9 m $\times$ 12 m. The classroom has some empty desks, resulting in a strong LoS scenario. The third environment is part of a library with a size of 7 m $\times$ 10 m. The library has many shelves which have a height of 2.5 m and are made of metal and wood, resulting in a rich multipath and strong NLoS scenario. Due to privacy concerns, we only present the testbed floorplan in Fig. 14. In each environment, the test locations are 0.6 m separated from each other, and a person with a height of 1.72 m acts as the target.

Hardware Configuration. In each environment, we deploy 11 laptops, each of them equipped with an Intel 5300 NIC. Four of the 11 laptops are modified to act as APs with the "hostapd" tool in [21] and the remaining 7 laptops act as clients. For all environments, the locations of APs, clients together with the test points are marked in Figs. 14a, 14b, and 14c, respectively. Each AP probes the other 3 APs and all the clients every 100 ms (a typical beacon transmission interval) to obtain CSI. A desktop with 3.6 GHz CPU (Intel i7-4790) and 8 GB memory is employed as the server to collect CSI measurements through wired connections and runs our localization algorithm.

Default Deployment Setup. In reality, the locations of APs and some clients are fixed and known. Thus, we assume the locations of all the 4 APs and one of the 7 clients are known in our experiments. Usually, most clients (such as laptops or mobiles) rest on a table or are held in the hand, so we set the heights of clients as 1.2 m off the ground. The heights of APs vary a lot. Some users like to place the APs on the wall which is higher than a table, while others still place the APs

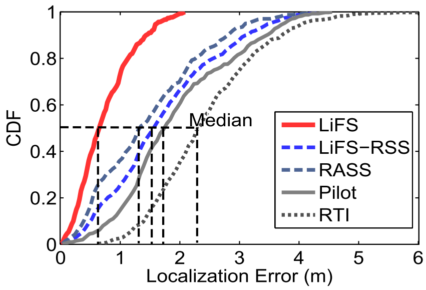

Fig. 15. CDF plot of the localization errors in home.

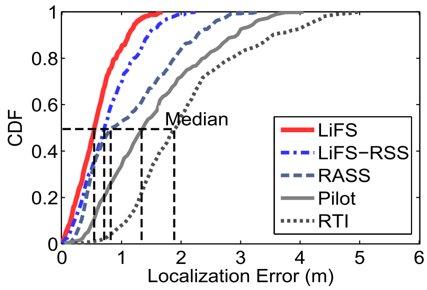

Fig. 16. CDF plot of the localization errors in classroom (strong LoS).

on the table. Thus, we place two APs at a height of 1.7 m above the ground and the rest two APs on the table with a height of 1.2 m. Unless specifically mentioned, we use the default setup introduced here for performance evaluation in the rest of this paper.

Experimental Methodology. LiFS has two phases. First is the baseline data acquisition when no target is present. Each pair of transceivers (consisted of an AP and a client) records 10 packets and forwards the packets to the server. Second is the localization phase. When a target moves into the monitoring area, each pair records 10 packets and also forwards the packets to the server. At the server side, LiFS pre-processes the CSI data and estimates the target's location by solving the power fading model equations. In order to eliminate the random errors, we run both LiFS and other localization schemes 40 times at each test location.

8 Performance Evaluation

8.1 Comparison and Metric

We compare LiFS with three other schemes in real indoor environments described in Section 7.

- *Pilot:* Pilot [14] is a state-of-the-art CSI-based device-free localization scheme utilizing the CSI correlations of all subcarriers as fingerprints. Pilot uses the kernel density-based maximum a posteriori probability (MAP) algorithm to localize a target. We find that Pilot performs the best when the kernel bandwidth is 3, and we use this setting in our experiments as well.
- *RASS:* RASS [6] is a power-based scheme which utilizes the RSS change, i.e., the averaged CSI amplitude changes over all subcarriers as fingerprints. RASS uses the support vector regression algorithm to localize a target. For a fair comparison, we use pre-processed CSI change measurements as the input for RASS and employ the "LIBSVM" tool [45] used in RASS to localize a target.
- *RTI:* RTI [5] does not need offline training effort, which has the similar advantage as LiFS. RTI requires the prior knowledge of all the transceivers' locations. For a fair comparison, we employ the scheme proposed in the well-known EZ [44] system to localize the unknown transceivers.

Performance Metric. Most human targets have a width of no larger than 40 cm. To calculate the localization error, we can not treat human target as a point. Thus, we consider there is no localization error as long as the estimation is within 20 cm range centred on the true location. Otherwise, the error is calculated as the minimum distance between the estimated location and this range area.

8.2 Overall Localization Accuracy

8.2.1 Localization Accuracy in Home Environment

We have the test subject go through all 107 test locations. Fig. 15 depicts the CDF plot of the localization errors. It shows that LiFS performs best with the median and 80-percentile errors as small as 0.7 m and 1.2 m, respectively. RASS, LiFS-RSS, Pilot and RTI yield larger median errors of 1.4 m, 1.5 m, 1.8 m and 2.4 m.

The poor performance of RTI is due to the fact that RTI needs precise locations of all the transceivers (i.e., APs and clients). The unknown transceivers' location errors caused by EZ would decrease the localization accuracy of RTI. Unlike RTI, LiFS can localize the target accurately without requiring to know all the transceivers' locations.

The performance of RASS and Pilot is not as good as LiFS since the CSI measurements vary over time [29]. Thus, the online measurements will not match the fingerprints in the database, resulting in large errors. Unlike RASS and Pilot, LiFS does not rely on manually-collected fingerprints. By modelling the pre-processed CSI measurements with the power fading model equations, LiFS has sufficient restrictions to localize the target accurately.

Compared with Pilot, the superiority of RASS stems from our CSI pre-processing scheme. The space distance of the pre-processed CSI data is larger than the raw CSI data as validated in Section 5.3. Thus, RASS with the pre-processed CSI data outperforms Pilot with the raw CSI data.

8.2.2 Evaluation in LoS and NLoS Scenarios

This section answers the two questions: First, what is the localization accuracy of LiFS in LoS and NLoS scenarios? Second, compared with RSS, how much accuracy has been improved by the pre-processed CSI? To answer the questions, we choose the open classroom environment and the library environment.

Figs. 16 and 17 show the localization errors for all the four schemes in LoS and NLoS scenarios. All the schemes perform better in LoS. Compared with LoS scenario, the median localization errors of LiFS, RASS, Pilot and RTI degrade by about 2×, 2.3×, 1.7× and 1.5× in NLoS, respectively. Overall, LiFS achieves 1.6×, 2.8× and 3.8× higher accuracies than RASS, Pilot and RTI in LoS, and 1.6×, 2.2× and 2.7× in NLoS.

The localization errors of LiFS using RSS in LoS and NLoS scenarios are also shown in Figs. 16 and 17. The

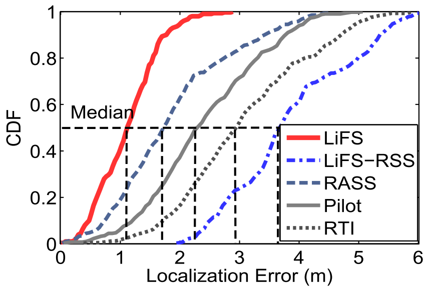

Fig. 17. CDF plot of the localization errors in library (strong NLoS).

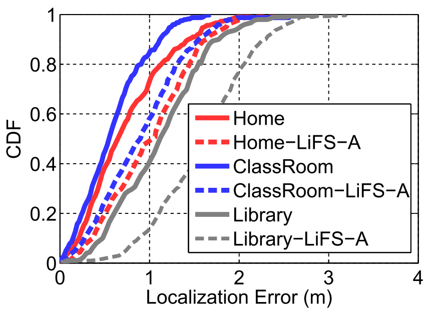

Fig. 18. Localization errors of LiFS and LiFS-A in different environments.

localization accuracy of LiFS using RSS is comparable to employing the pre-processed CSI in LoS. The reason is that the RSS values match the model relatively well in LoS because of little and weak multipath. In contrast, when there is rich multipath in the NLoS scenario, only a few subcarriers' CSI amplitudes match the proposed model. RSS is an averaged "CSI amplitude" over all subcarriers [20], [29]. Consequently, the RSS values do not match the model, and LiFS with RSS suffers large errors in the NLoS scenario.

8.2.3 Comparisons between LiFS and LiFS-A

Here, we compare the localization accuracy of LiFS and LiFS-A in the three different environments. The results in Fig. 18 show that the accuracy of LiFS-A decreases slightly compared with the localization accuracy of LiFS. The median localization errors of LiFS-A and LiFS are 1.06 m and 0.7 m in the home environment. The decreased accuracy of LiFS-A is due to the approximated fresnel integration, which leads to larger difference between model-calculated CSI values and the pre-processed CSI measurements.

8.3 Performance under Different Parameters

8.3.1 Impact of the Number of Clients

To examine the impact of the number of clients on LiFS' performance, we increase the number of clients from 5 to 21 with a step size of 2, while only one client's location is known. As illustrated in Fig. 19, it is apparent that the average localization errors of all the schemes become smaller with more clients deployed. The intuition is that, with more clients, LiFS (including other systems) has more constraints on a target's location. Note that, the amount of accuracy improvement is very limited when the number of clients is more than 15. LiFS and LiFS-A always outperform the other three schemes.

8.3.2 Impact of the Fraction of Known Clients

If more clients' locations become available, we would expect LiFS' performance to be improved. To evaluate this, we

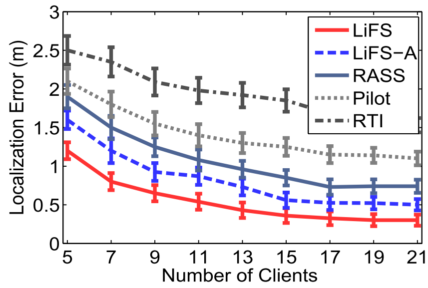

Fig. 19. Impact of the number of clients.

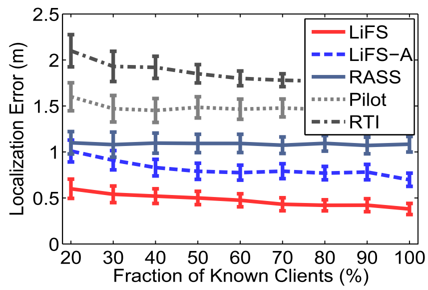

Fig. 20. Impact of the fraction of known location clients.

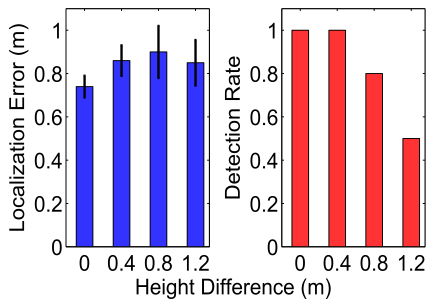

Fig. 21. Impact of the AP-client height difference.

employ 10 clients and increase the fraction of clients with known locations from 20 to 100 percent with a step size of 10 percent. Fig. 20 shows that the localization errors of LiFS, LiFS-A and RTI decrease with the increased fraction of known-location clients. We attribute the improvement to the following reasons. The localization accuracy of LiFS, LiFS-A and RTI is related to the location precision of the clients. With more clients knowing their precise locations, less errors would be added into the target's location estimation. However, we can see that LiFS' performance is not affected much even very few clients' locations are known. For RASS and Pilot, their localization errors are almost unchanged with the increase of the number of known clients. The reason is that RASS and Pilot are "training and matching" based schemes, which do not rely on the clients' locations [6], [14].

8.3.3 Impact of AP-Client Height Difference

In reality, APs and most clients are not placed at the same height. We seek to study whether this height difference would cause large location errors. To do so, we place all the clients on several desks which are 1.2 m above the ground. Then, we simultaneously increase the heights of all APs from 1.2 m to 2.4 m with a step size of 0.4 m. In Fig. 21, the right subgraph shows the detection rate and the left subgraph shows the localization error. The detection rate is defined as the number of locations can be localized divided

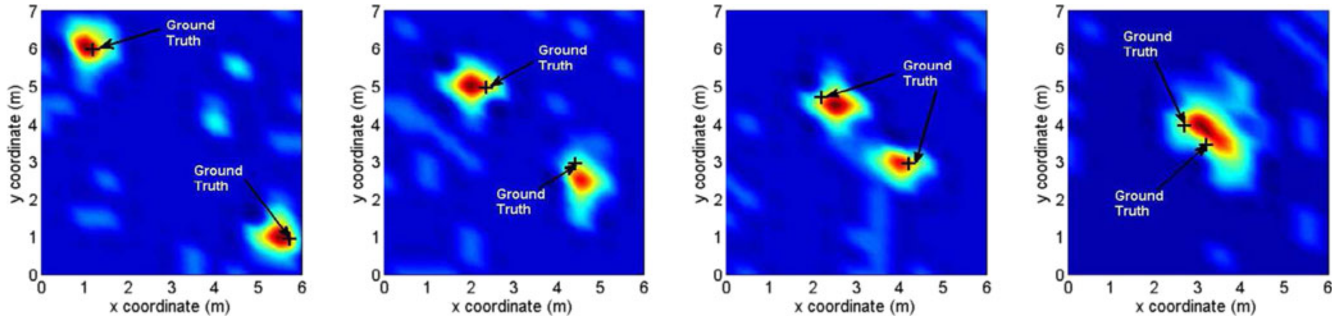

Fig. 22. Four snapshot localization results when two targets are 5.4 m, 3 m, 1.8 m, and 0.6 m apart, respectively.

by the total number of test locations. Fig. 21 shows that the detection rate is decreased with the increase of height difference. Since, when an AP is placed much higher than a target, the target's effect on the wireless link is very small and thus may not be detected. When the height difference is below 0.8 m which is commonly seen in reality, the detection rate achieved is no less than 80 percent.

For a given height difference setting, we only include those test locations at which a target can be detected for localization performance evaluation. Fig. 21 shows that the localization error of LiFS is always less than 1 m no matter what height the APs are placed, since LiFS can estimate the unknown height difference together with the target location.

8.4 Two-Target Localization

Here, we discuss the performance of LiFS for localizing two targets. The intuition is that a target is not able to affect all the wireless links simultaneously. When two targets are located sparsely, each target will affect a disjoint subset of links and thus can be separated and individually located. However, when many targets exist or two targets are very close to each other, it's still challenging to accurately localize each of them.

We conduct experiments in the "Living room" of the home setting (Fig. 14a) with a size of 7 m $\times$ 6 m. Two persons with heights of 171 cm and 173 cm act as the targets. We let one target move from the top left corner to the lower right corner, and the other target move from the lower right corner to the top left corner simultaneously. Fig. 22 shows four snapshot localization results when the two targets are 5.4 m, 3 m, 1.8 m and 0.6 m away from each other. For each snapshot, we collect 30 measurements and the localization results are mapped into the heatmaps, where the red dots represent the estimated locations and the plus signs indicate the ground truths. LiFS is able to localize the two targets when they are located sparsely. However, when the two targets are close to each other, LiFS has difficulties localizing each individual and we leave this challenging problem as our future work.

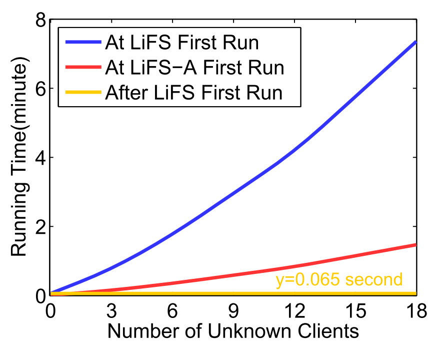

Fig. 23. Running time cost.

8.5 System Latency

To demonstrate running time cost of LiFS and LiFS-A, we increase the number of unknown clients from 0 to 18, and a total number of 21 clients are deployed. Fig. 23 shows the running time results for localizing a target. When we run LiFS and LiFS-A at the first time, the running time increases with more unknown clients. Fig. 23 clearly shows that (i) the time cost of the LiFS-A decreases 80 percent compared with LiFS; (ii) the running time significantly decreases to 0.065 s after the system's first run, since we only need to estimate the location of the target.

9 Conclusion

LiFS is a model-based device-free localization system that does not require any explicit pre-deployment effort or exhaustive fingerprint collection. We design, implement and evaluate LiFS against the existing Pilot, RASS and RTI systems. Real-world experiments demonstrate that LiFS outperforms the three state-of-the-art systems.

Acknowledgments

This work is supported in part by the National Natural Science Foundation of China under Grants (61572402, 61732017, 61672428, 61772422, 61572219), and by the National Science Foundation under Grant No. 1617161.

References

[1] J. Xiong, K. Sundaresan, and K. Jamieson, "Tonetrack: Leveraging frequency-agile radios for time-based indoor wireless localization," in *Proc. 21st Annu. Int. Conf. Mobile Comput. Netw.*, 2015, pp. 537–549.

[2] J. Xiong and K. Jamieson, "Arraytrack: A fine-grained indoor location system," in *Pro. 10th USENIX Conf. Netw. Syst. Des. Implementation*, 2013, pp. 71–84.

[3] Y. Shu, K. G. Shin, T. He, and J. Chen, "Last-mile navigation using smartphones," in *Proc. 21st Annu. Int. Conf. Mobile Comput. Netwo.*, 2015, pp. 512–524.

[4] A. Achtzehn, L. Simic, P. Gronerth, and P. Mahonen, "A propagation-centric transmitter localization method for deriving the spatial structure of opportunistic wireless networks," in *Proc. IEEE Conf. Wireless On-Demand Netw. Syst. Serv.* , 2013, pp. 139–146.

[5] J. Wilson and N. Patwari, "See-through walls: Motion tracking using variance-based radio tomography networks," *IEEE Trans. Mobile Comput.*, vol. 10, no. 5, pp. 612–621, May 2011.

[6] D. Zhang, Y. Liu, X. Guo, and L. M. Ni, “Rass: A real-time, accurate, and scalable system for tracking transceiver-free objects,” *IEEE Trans. Parallel Distrib. Syst.*, vol. 24, no. 5, pp. 996–1008, May 2013.
[7] F. G. Miskelly, “Assistive technology in elderly care,” *Age Ageing*, vol. 30, no. 6, pp. 455–458, 2001.
[8] F. Adib, Z. Kabelac, and D. Katabi, “Multi-person localization via rf body reflections,” in *Proc. 12th USENIX Symp. Netw. Syst. Des. Implementation*, 2015, pp. 279–292.
[9] L. Yang, Q. Lin, X. Li, T. Liu, and Y. Liu, “See through walls with cots rfid system!,” in *Proc. ACM 21st Annu. Int. Conf. Mobile Comput. Netw.*, 2015, pp. 1–12.
[10] J. Wang, Q. Gao, P. Cheng, Y. Yu, K. Xin, and H. Wang, “Lightweight robust device-free localization in wireless networks,” *IEEE Trans. Ind. Electron.*, vol. 61, no. 10, pp. 5681–5689, Oct. 2014.
[11] S. Nannuru, Y. Li, Y. Zeng, M. Coates, and B. Yang, “Radio-frequency tomography for passive indoor multitarget tracking,” *IEEE Trans. Mobile Comput.*, vol. 12, no. 12, pp. 2322–2333, Dec. 2013.
[12] M. Youssef, M. Mah, and A. Agrawala, “Challenges: Device-free passive localization for wireless environments,” in *Proc. 13th Annu. ACM Int. Conf. Mobile Comput. Netw.*, 2007, pp. 222–229.
[13] J. Wang, B. Xie, D. Fang, X. Chen, C. Liu, T. Xing, and W. Nie, “Accurate device-free localization with little human cost,” in *Proc. ACM Int. Workshop Experiences Des. Implementation Smart Objects*, 2015, pp. 55–60.
[14] J. Xiao, K. Wu, Y. Yi, L. Wang, and L. M. Ni, “Pilot: Passive device-free indoor localization using channel state information,” in *Proc. IEEE Int. Conf. Distrib. Comput. Syst.* , 2013, pp. 236–245.
[15] W. Yang, L. Gong, D. Man, J. Lv, H. Cai, X. Zhou, and Z. Yang, “Enhancing the performance of indoor device-free passive localization,” *Int. J. Distrib. Sensor Netw.*, vol. 2015, no. 4, pp. 1–11, 2015.
[16] Y. Wang, J. Liu, Y. Chen, M. Gruteser, J. Yang, and H. Liu, “E-eyes: Device-free location-oriented activity identification using fine-grained wifi signatures,” in *Proc. 20th Annu. Int. Conf. Mobile Comput. Netw.*, 2014, pp. 617–628.
[17] A. F. Molisch, *Wireless Communications*. Hoboken, NJ, USA: Wiley.
[18] T. Mcconaghy, E. Vladislavleva, and R. Riolo, “Genetic programming theory & practice,” in *Proc. Annu. Genetic Evol. Comput. Conf. Gecco Companion Publication* , pp. 3015–3056, vol. 78, 2010.
[19] M. S. Bazaraa, H. D. Sherali, and C. M. Shetty, *Nonlinear Programming: Theory and Algorithms*. Hoboken, NJ, USA: Wiley.
[20] H. Daniel, H. Wenjun, S. Anmol, and W. David, “Linux 802.11n csi tool,” (2011). [Online]. Available: dhalperi.github.io/linux-80211n-csitool/faq.html
[21] J. Malinen, et al., “hostapd: Ieee 802.11 ap, ieee 802.1 x,” Tech. Rep., *WPA/WPA2/EAP/RADIUS Authenticator*, (2013). [Online]. Available: hostap.epitest.fi/hostapd
[22] H. Ma, C. Zeng, and C. X. Ling, “A reliable people counting system via multiple cameras,” *ACM Trans. Intell. Syst. Technol.*, vol. 3, no. 2, 2012, Art. no. 31.
[23] J. Kemper and D. Hauschildt, “Passive infrared localization with a probability hypothesis density filter,” in *Proc. IEEE Workshop Positioning Navigation Commun.*, 2010, pp. 68–76.
[24] F. Adib and D. Katabi, “See through walls with wifi!,” in *Proc. ACM SIGCOMM*, 2013, pp. 75–86.
[25] K. Joshi, D. Bharadia, M. Kotaru, and S. Katti, “Wideo: Fine-grained device-free motion tracing using rf backscatter,” in *Proc. 12th USENIX Symp. Netw. Syst. Des. Implementation* , 2015, pp. 189–204.
[26] T. Wei and X. Zhang, “mtrack: High-precision passive tracking using millimeter wave radios,” in *Proc. 21st Annu. Int. Conf. Mobile Comput. Netw.*, 2015, pp. 117–129.
[27] I. Sabek, M. Youssef, and A. V. Vasilakos, “Ace: An accurate and efficient multi-entity device-free wlan localization system,” *IEEE Trans. Mobile Comput.*, vol. 14, no. 2, pp. 261–273, Feb. 2015.
[28] Y. Guo, K. Huang, N. Jiang, X. Guo, Y. Li, and G. Wang, “An exponential-rayleigh model for RSS-based device-free localization and tracking,” *IEEE Trans. Mobile Comput.*, vol. 14, no. 3, pp. 484–494, Mar. 2015.
[29] D. Halperin, W. Hu, A. Sheth, and D. Wetherall, “Predictable 802.11 packet delivery from wireless channel measurements,” in *Proc. ACM SIGCOMM*, 2011, pp. 159–170.
[30] K. Wu, J. Xiao, Y. Yi, M. Gao, and L. M. Ni, “Fila: Fine-grained indoor localization,” in *Proc. IEEE INFOCOM*, 2012, pp. 2210–2218.
[31] C. Xu, B. Firner, Y. Zhang, and R. Howard, “The case for efficient and robust rf-based device-free localization,” *IEEE Trans. Mobile Comput.*, vol. 15, no. 9, pp. 2362–2375, Sep. 2016.
[32] Z. Zhou, Z. Yang, C. Wu, L. Shangguan, and Y. Liu, “Towards omnidirectional passive human detection,” in *Proc. IEEE INFOCOM*, 2013, pp. 3057–3065.
[33] J. Wang, H. Jiang, J. Xiong, K. Jamieson, X. Chen, D. Fang, and B. Xie, “Lifs: Low human-effort, device-free localization with fine-grained subcarrier information,” in *Proc. 22nd Annu. Int. Conf. Mobile Comput. Netw.*, 2016, pp. 243–256.
[34] J. Wang, L. Zhang, X. Wang, J. Xiong, X. Chen, and D. Fang, “A novel csi pre-processing scheme for device-free localization indoors,” in *Proc. 8th Wireless Students Students Students Workshop*, 2016, pp. 6–8.
[35] R. v. Nee and R. Prasad, *OFDM for Wireless Multimedia Communications*. Norwood, MA USA: Artech House.
[36] W. Shen, K. C. Lin, S. Gollakota, and M. Chen, “Rate adaptation for 802.11 multiuser mimo networks,” *IEEE Trans. Mobile Comput.*, vol. 13, no. 1, pp. 35–47, Jan. 2014.
[37] W. C. Y. Lee, *Mobile Communication Engineering*., New York, NY, USA: McGraw Hill, 1985.
[38] D. Halperin, W. Hu, A. Sheth, and D. Wetherall, “Tool release: Gathering 802.11 n traces with channel state information,” *ACM SIGCOMM Comput. Commun. Rev.*, vol. 41, no. 1, pp. 53–53, 2011.
[39] J. Wang, D. Fang, Z. Yang, H. Jiang, X. Chen, T. Xing, and L. Cai, “E-hipa: An energy-efficient framework for high-precision multi-target-adaptive device-free localization,” *IEEE Trans. Mobile Comput.*, vol. 12, no. 5, pp. 1–12, May 2016.
[40] J. Wang, X. Chen, D. Fang, C. Q. Wu, Z. Yang, and T. Xing, “Transferring compressive-sensing-based device-free localization across target diversity,” *IEEE Trans. Ind. Electron.*, vol. 62, no. 4, pp. 2397–2409, Apr. 2015.
[41] Y. Xie, Z. Li, and M. Li, “Precise power delay profiling with commodity wifi,” in *Proc. 21st Annu. Int. Conf. Mobile Comput. Netw.*, 2015, pp. 53–64.
[42] J. Wang and D. Katabi, “Dude, where’s my card? rfid positioning that works with multipath and non-line of sight,” in *Proc. ACM SIGCOMM*, 2013, pp. 51–62.
[43] S. Salvador and P. Chan, “Toward accurate dynamic time warping in linear time and space,” *Intell. Data Anal.*, vol. 11, no. 5, pp. 561–580, 2007.
[44] K. Chintalapudi, A. P. Iyer, and V. N. Padmanabhan, “Indoor localization without the pain,” in *Proc. 16th Annu. Int. Conf. Mobile Comput. Netw.*, 2010, pp. 173–184.
[45] LIBSVM, “Library to using svm.” (2016). [Online]. Available: www.csie.ntu.edu.tw/cjlin/libsvm/

Ju Wang received the BS and PhD degrees from the School of Information Science and Technology, Northwest University, China, in 2011 and 2017, respectively. Now, he is a postdoctoral fellow in the Cheriton School of Computer Science, University of Waterloo. His research interests include localization, RF-based sensing and signal processing for smart city.

Jie Xiong received the PhD degree from University College London, in 2015. He is an assistant professor in the College of information and Computer Sciences, UMass Amherst. He was awarded the prestigious Google European Doctoral Fellowship in Wireless Networking for his doctoral studies. His PhD thesis won the 2016 British Computer Society Distinguished Dissertation Award runner-up. He has broad research interests include building practical wireless and mobile systems that bridge the gaps between theory and reality. His recent work appeared at MobiCom, NSDI, UbiComp, and INFOCOM and won the CoNEXT ’14 Best Paper Award.

Hongbo Jiang received the PhD degree from Case Western Reserve University, in 2008. After that, he joined the faculty of the Huazhong University of Science and Technology as a full professor and the dean of the Department of Communication Engineering. Now, he is a full professor in the College of Computer Science and Electronic Engineering, Hunan University. His research concerns computer networking, especially algorithms and protocols for wireless and mobile networks. He is serving as the editor for the *IEEE/ACM Transactions on Networking*, the associate editor for the *IEEE Transactions on Mobile Computing*, and the associate technical editor for the I*EEE Communications Magazine*. He is a senior member of the IEEE.

Kyle Jamieson received the BS and MEng degrees in computer science from the Massachusetts Institute of Technology, and the PhD degree in computer science from the Massachusetts Institute of Technology, in 2008. He is an associate professor with the Department of Computer Science, Princeton University and honorary (adjunct) reader of wireless systems and networks, University College London. His research interests include building wirelessly networked systems for the real world that cut across the boundaries of digital communications and networking. He then received a Starting Investigator fellowship from the European Research Council, in 2011, Best Paper awards at USENIX 2013 and CoNEXT 2014, and a Google Faculty Research Award in 2015.

Xiaojiang Chen received the PhD degree in computer software and theory from Northwest University, Xi'an, China, in 2010. He is currently a professor with the School of Information Science and Technology, Northwest University. His current research interests include RF-based sensing and performance issues in Internet of things.

Dingyi Fang received the BS and MS degrees in computer science from Northwest University, Xi'an, China, in 1983 and 1988, respectively, and the PhD degree in computer application technology from Northwestern Polytechnical University of China, in 2001. He is currently a professor with the School of Information Science and Technology, Northwest University, Xi'an, China. His current research interests include mobile and distributed computing systems, network and information security, and wireless sensor networks.

Chen Wang received the BS and PhD degrees from the Department of Automation, Wuhan University, China, in 2008 and 2013, respectively. From 2013 to 2017, he was a postdoctoral research fellow in the Networked and Communication Systems Research Lab, Huazhong University of Science and Technology, China. Thereafter, he joined the faculty of the Huazhong University of Science and Technology where he is currently an associate professor. His research interests include the broad areas of wireless networking, Internet of Things, and mobile computing, with a recent focus on privacy issues in wireless and mobile systems. He is a member of the IEEE.